Biomedical Signal Processing and Control 71 (2022) 103092

Contents lists available at ScienceDirect

Biomedical Signal Processing and Control

journal homepage: www.elsevier.com/locate/bspc

The intracranial Windkessel implies arteriovenous pulsatile coupling increased by venous resistances

Giuseppe Baselli [a], Maria Marcella Laganà [b,*]

[a] Department of Electronics, Information, and Bioengineering, Politecnico di Milano, Milano, Italy
[b] IRCCS Fondazione Don Carlo Gnocchi ONLUS, Milan, Italy

ARTICLE INFO

Keywords:
Lumped-parameter model
Cerebrovascular circulation
Rehabilitation
Neurodegeneration
Venous pulsatility
Venous insufficiency

ABSTRACT

Various detailed models of cerebral circulation have been proposed, recently fostered by the hypothesized relationship between extracranial venous drainage impairment and neurodegenerative diseases. However, some basic model is missing, analogous to the 2-element Windkessel (WK) of the systemic circulation. This theoretical study focuses, in the simplest way, on the dependence of intracranial venous pressure (VP) pulsatility on the intracranial arterial 2-element WK and the venous resistance R_V. The WK compliance is shown to exert an arteriovenous capacitive coupling (AV-CC), agumented by R_V increments. The WK was estimated based on the intracranial arterial pressure (AP) and flow (Φ_{ICA}) waves of an open database of 3325 virtual subjects. A normal R_V was estimated imposing a mean VP of 10 mmHg, doubled to mimic hindered extracranial veins. The AP to VP transfer function showed: i) a gain almost proportional to R_V; ii) a zero slightly below heart rate (HR) corresponding to the arterial WK pole; iii) a mid-frequency derivative band up to the AV-CC pole, the frequency of which was almost inversely proportional to R_V; iv) full coupling at high frequencies, yet above the pulse harmonic content, at normal HR. In conclusion, besides the well-known effect of venous hindering on the mean VP, the results of this model support the hypothesis that abnormal pulsatility of cerebral veins may play a significant role in cerebrovascular imbalance and related neurodegeneration.

1. Introduction

Over the last decade, intracranial (IC) venous circulation has gained further interest due to published evidence of a link between anomalies of the venous extracranial routes and various clinical conditions [1], such as idiopathic normal pressure hydrocephalus [2], idiopathic IC hypertension [3], transient global amnesia [4], Meniere's disease [5], Parkinson's Disease [6], and multiple sclerosis [7,8]. Hence, several studies addressed chronic cerebrospinal venous insufficiency and other anatomical or functional venous anomalies [6,9,10].

In this perspective, the present theoretical study addresses a highly simplified model in order to provide easy comprehension of hindered venous outflow (Φ_{ICV}) effects on IC venous pressure (VP) pulsatility. The adopted approach recalls that of the Windkessel (WK) model [11] of the systemic arterial pulse. It is classical knowledge that the WK is presented with increasing degrees of complexity (i.e., number of lumped elements), depending on specific applications. Even the minimal version of the 2-element WK [12] provides immediate insight over major features of arterial pressure (AP) wave shaping, yet not denying higher complexity levels addressed by adding further structure and model elements [13,14].

Similar to the other arterial compartments, the IC one is known to display a WK effect, which smooths the arterial flow (Φ_{ICA}) pulse, and supports circulation during diastole [15]. The mechanisms of this phenomenon have been modelled for decades and consist of a closed Φ_{ICA} interaction with venous and cerebrospinal fluid (CSF) flows [16,17]. In

Abbreviations: AP, arterial pressure (P_{ICA} in equations); AV, arteriovenous; AV-CC, arteriovenous capacitive coupling; CSF, cerebrospinal fluid; C_{ICA}, compliance of IC arteries; C_{ICV}, venous compliance; DAP, diastolic arterial pressure; Φ_{ICA}, arterial flow; Φ_{ICV}, venous outflow; G_{AV}, gain from mean arterial pressure and mean venous pressure; HP, heart period; HR, heart rate; IC, Intracranial; MAP, median arterial pressure; MFL, median flow; p_{av}, arteriovenous capacitive coupling pole; R_{IC}, peripheral IC resistances; R_V, venous resistance; $R_V\uparrow$, increased R_V; $R_V\downarrow$, decreased R_V; SAP, systolic arterial pressure; τ_{av}, time constant from arterial flow to venous pressure; TF, transfer function; τ_{Wk}, WK time constant; VP, venous pressure (P_{ICV} in equations); WK, Windkessel; z_{wk}, arterial WK pole, and zero of the arteriovenous coupling transfer function.

* Corresponding author: Maria Marcella Laganà, Via Capecelatro, 66, Milan 20148, Italy.
E-mail address: mlagana@dongnocchi.it (M.M. Laganà).

https://doi.org/10.1016/j.bspc.2021.103092
Received 29 October 2020; Received in revised form 30 July 2021; Accepted 20 August 2021
Available online 2 September 2021

the last decades, studies regarding IC circulation and the temporal relationships between arterial, venous and CSF flows gained a new, quantitative, and non-invasive tool thanks to Phase-Contrast Magnetic Resonance Imaging. Using this technique, the arterial, venous and CSF flows can be quantified [18–20].

The characteristics of the IC circulation are determined by the confined skull volume filled by incompressible fluids and tissues. As stated by the Monroe-Kelly hypothesis [7], this constraint imposes an instantaneous balance of arterial and venous blood volume (and also CSF, yet neglected here for the sake of simplicity). For this reason we had to include at least an arteriovenous (AV) capacitive coupling (AV-CC) in our model (Fig. 1A). So, in contrast with the WK descriptions of other regions, usually neglecting the venous compartment, the venous resistance (R_V) gains a central role for the IC region (Fig. 1A). Indeed, it hinders the mentioned compensation, with a dynamic effect superimposed to the trivial increment of mean VP.

Several mathematical, physical, and computer simulation models of the IC circulation have also been proposed for a better understanding of the interplay of AP, VP, CSF, and IC pressure, with impact on various clinical applications [3,17,21–28]. Further, a variety of studies focused how extra-cranial venous alterations impact the IC fluid dynamics and pressures [24,25,27,29–31].

The simple theoretical model proposed in the current study addresses the frequency response of the AV-CC system and its relationship with the arterial pulse harmonics, thus highlighting the interplay of heart rate (HR) and the dynamic response of the IC circulation.

Some of the concepts here developed were shortly described in our previous study [32], which qualitatively considered the AV-CC but lacked any quantification of its dynamics. The current study, conversely, provides a complete description of the proposed model and the consequent AP to VP transfer function (TF), preliminarily described in [33]. In the current study, the IC WK parameters were estimated through a database of virtual subjects [34]. The potential usefulness of this approach relies on a basic understanding of how increased R_V ($R_V\uparrow$) might affect the IC components driving the WK and AV-CC mechanisms.

2. Methods

2.1. Minimal lumped intracranial pulse model

A qualitative sketch of our simplified model is shown in Fig. 1A, which represents the mean IC flow (open black arrows) and the superimposed pulse. The arrows representing pulsatility are pointed in the systolic direction, i.e., Φ_{ICA} and Φ_{ICV} peaks. The left side shows the arterial compartment, represented by a lumped compliance of IC arteries (C_{ICA}) which runoff into the peripheral IC resistances (R_{IC}). The arterial pulse (upward red arrow) is shaped by the usual WK mechanism.

However, according to the Monroe-Kelly hypothesis of virtually incompressible IC tissues and fluids, each expansion of C_{ICA} (rightward red arrow) implies a venous compression pulse (rightward blue arrow). Remarkably, such pulse is discharged on a reduced resistance (i.e., the parallel of R_V and R_{IC}), which in turn reduces the pulsatility ΔP_{IC}. Though countercurrent, the evidenced "back-pulse" to R_{IC} is the physiological consequence of R_V and does not imply a negative flow, but a transient effect on the vascular bed flow, opposed to that of the AP pulse.

Fig. 1B represents, by an electrical analog, the previously described lumped model. By hypothesizing the venous compliance satisfies the condition $C_{ICV} \gg C_{ICA}$, it is thus assimilated to a short circuit, permitting to quantify both the WK and the AV-CC upon C_{ICA} only (see next paragraph, 2.2). The "Model limitations" paragraph of the Discussion details all simplified and neglected mechanisms relevant to the interplay of CSF circulation and dynamics with the compartments of IC veins and sinuses and the relevant complex structures herein lumped into single compartments.

2.2. Lumped model transfer function analysis

The input impedance describes the 2-element arterial WK:

$$Z_{ICA}(s) = \frac{P_{ICA}(s)}{\Phi_{ICA}(s)} = \frac{R_{IC}}{sR_{IC}C_{ICA} + 1} \tag{1}$$

where $R_{IC}C_{ICA} = \tau_{WK}$ is the WK time constant. This TF was identified on a large virtual database in order to quantify both R_{IC} and C_{ICA} (see next paragraph, 2.3).

Most of the results and discussion will address the TF from AP

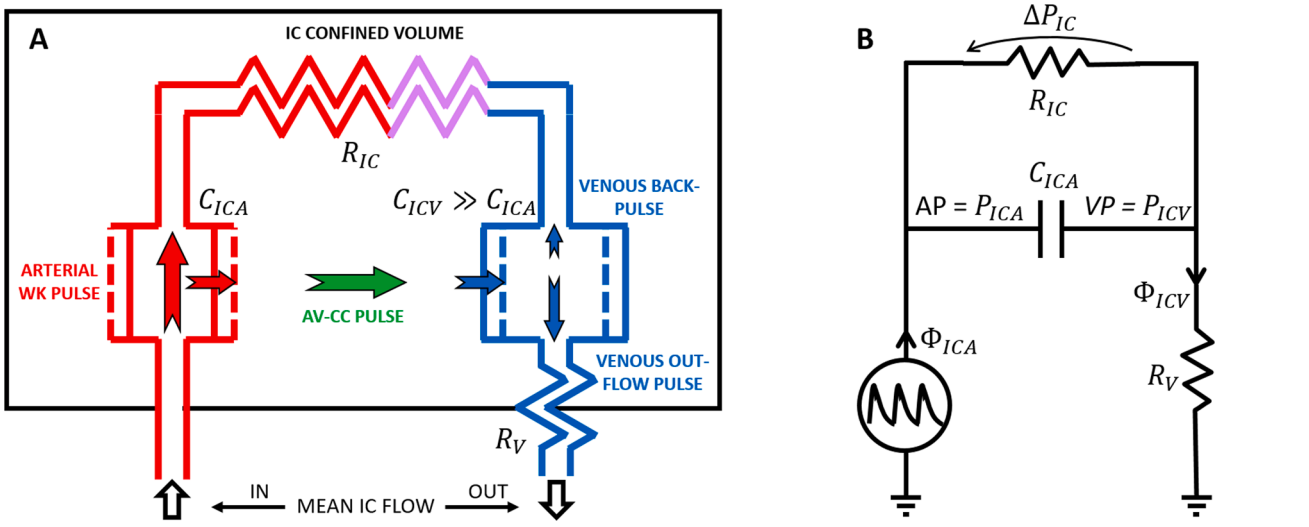

Fig. 1. A) Qualitative scheme of the pulsating volume exchanges (colored arrows shown in the systolic phase) superimposed to mean flow (open arrows): the Windkessel (WK) arterial pulse (upward red arrow) directed to the IC vascular bed resistances R_{IC} also causes an expansion of the IC arterial compliances C_{ICA} (rightward red arrow) and, via the arteriovenous capacitive coupling (AV-CC, green), compression of the venous compliances C_{ICV} (rightward blue arrow). The consequent venous pressure (VP) pulse is split in an outflow pulse, hindered by venous resistances R_V, and in a back-pulse. B) The hyper-simplified lumped model is shown by its electrical analog; hypothesizing $C_{ICV} \gg C_{ICA}$, the former is assimilated to a short circuit and accordingly omitted; the pulsatile arterial inflow $\Phi_{ICA}(t)$ and pressure AP $= P_{ICA}(t)$ are evidenced as well as the venous outflow $\Phi_{ICV}(t)$ and pressure VP $= P_{ICV}(t)$. The pulsatile pressure drop across R_{IC}, $\Delta P_{IC}(t)$, is also evidenced.

(symbol P_{ICA}) to VP (symbol P_{ICV}), which is:

$$\frac{P_{ICV}(s)}{P_{ICA}(s)} = \frac{R_V}{R_{IC}+R_V}\,\frac{sR_{IC}C_{ICA}+1}{s(R_V||R_{IC})C_{ICA}+1} = G_{AV}\frac{s\tau_{WK}+1}{s\tau_{AV}+1} = \frac{s-z_{WK}}{s-p_{AV}} \tag{2}$$

where $G_{AV} = R_V/(R_{IC}+R_V)$ is the direct current (DC, i.e., 0 Hz) gain between mean AP and mean VP and is almost proportional to R_V, since $R_{IC} \gg R_V$; $\tau_{AV} = (R_V||R_{IC})C_{ICA} = -(2\pi p_{AV})^{-1}$ (frequencies are in Hz), since the AV-CC displacement flow is discharged on the parallel $(R_V||R_{IC})$of R_V (outward) and the IC vascular bed (backward). Remarkably, in this context where $P_{ICA}(s)$ changes its role from the output of the WK impedance $Z_{ICA}(s)$ to input of the AV-CC TF, the WK pole appears as a zero with $\tau_{WK} = R_{IC}C_{ICA} = -(2\pi z_{WK})^{-1}$. Henceforth, the "WK pole" will be labelled as a zero z_{WK}, given the central role of the AP to VP TF.

Clearly, $|z_{WK}| < |p_{AV}|$, since $R_{IC} > (R_V||R_{IC})$. Thus, a derivative mid-frequency band (MFB) is predicted, where amplitude rises from G_{AV} in the low-frequency band (LFB) to the high-frequency band (HFB) asymptotic value. The latter equals 1 (0 dB), as evidenced by the zero-pole-k TF representation at the right end of (2).

A qualitative asymptotic Bode diagram is shown in Fig. 2, evidencing: i) the LFB, where pulse harmonics share the DC gain; ii) a derivative MFB between $|z_{WK}|$ and $|p_{AV}|$ with a slope of +20dB/dec and anticipating phase; iii) an HFB in which arterial pulse harmonics (if any) would be fully transmitted.

The VP anticipated phase in the MFB is counterintuitive and apparently conflicts with the AP → VP causality. The question is readily solved by acknowledging that the Φ_{ICA} is the real system input. The causal effect Φ_{ICA} → AP is delayed by a time constant τ_{WK}, while Φ_{ICA} → VP by the shorter time constant τ_{AV}. The delay mismatch is unveiled in the MFB where τ_{WK} is effective and τ_{AV} is not.

The pulse pressure-drop across R_{IC}, $\Delta P_{IC} = P_{ICA} - P_{ICV}$ was also studied in order to gain insight into possible perfusion reductions due to the VP counter-pulsation.

So, using the zero-pole-k form in (2), we obtained:

$$\frac{\Delta P_{IC}(s)}{P_{ICA}(s)} = 1 - \frac{s-z_{WK}}{s-p_{AV}} = \frac{z_{WK}-p_{AV}}{s-p_{AV}} = \frac{1-G_{AV}}{s\tau_{AV}+1} \tag{3}$$

The steady-state gain $(1-G_{AV})$ reflects mean AP partition on the R_{IC} and R_V series. More importantly, the zero is cancelled and the pulsatility across R_{IC} drops by 20 dB/Dec after the AV-CC pole, which might dampen pulse harmonics either with increased HR or with $R_V\uparrow$. In the linear context of the presented model, dampened pulsatility would not affect mean flow (i.e., brain perfusion), which depends on mean AP minus mean VP. Nonetheless, non-linear vascular bed models [35] show the favorable effect of pulsatility on peripheral perfusion with a decrease of the apparent R_{IC} with increased pulsatility.

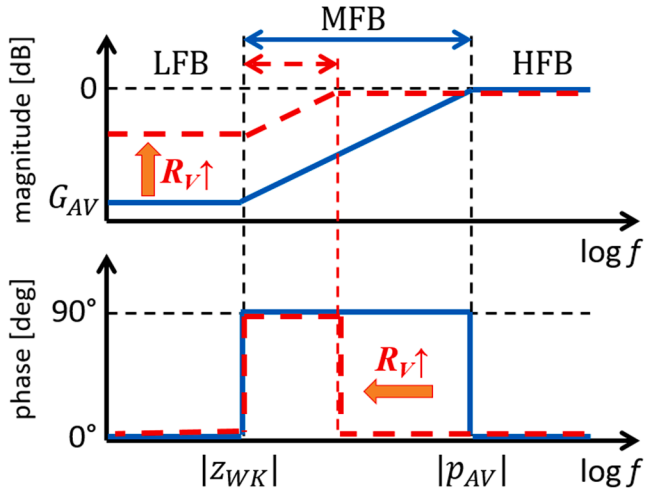

Fig. 2. Qualitative amplitude (top panel) and phase (bottom panel) characteristics of the transfer function from arterial to venous pressures. Effects of incremented venous resistance $R_V\uparrow$ (red) are compared to normal R_V (blue); p_{AV}=arteriovenous capacitive coupling pole; z_{WK} = IC WK pole assuming the role of a zero; f = frequency [Hz].

Time-domain simulations were performed starting from $\Phi_{ICA}(t)$ waveforms, so TFs from this entry deserves a brief presentation:

$$\frac{P_{ICV}(s)}{\Phi_{ICA}(s)} = Z_{ICA}(s)\frac{P_{ICV}(s)}{P_{ICA}(s)} = \frac{1}{C_{ICA}(s-p_{AV})} \tag{4}$$

$$\frac{\Delta P_{IC}(s)}{\Phi_{ICA}(s)} = Z_{ICA}(s)\frac{\Delta P_{IC}(s)}{P_{ICA}(s)} = \frac{1-G_{AV}}{C_{ICA}\tau_{AV}(s-z_{WK})(s-p_{AV})} \tag{5}$$

Interestingly, starting from the Φ_{ICA} wave: AP (1) is low-pass filtered by z_{WK} (classical WK effect), VP (4) by p_{AV}, and ΔP_{IC} (5) by both, thus experiencing both WK and AV-CC filtering.

2.3. Model parameter estimation

The estimation of $Z_{WK}(s)$ TF parameters (R_{IC} and C_{ICA}) was carried out exploiting an open database of simulations in the arterial tree of 3325 virtual subjects [34], which reports Φ_{ICA} and AP pulse waves in the main arterial branches up to the common carotid artery (CCA).

A scale adjustment was required to calibrate the total bilateral Φ_{ICA}, since the database does not separate the extracranial flow (external carotid arteries, ECA) from the IC flow (internal carotid arteries, ICA, and vertebral arteries, VA). Reference was made to the seminal measures reported by Schöning et al. [36] based on sonography in the CCA, ICA, VA, ECA. The reported monolateral values (mean±std) in ml/min are: CCA 470±120, ICA 265±62, ECA 160±66, VA 85±33. To this data corresponded the following bilateral mean values in ml/s: CCA 15.7, ICA 8.8, VA 2.8, ICA + VA 11.7, ECA 5.3. Our first working hypothesis was to correct the bilateral CCA flow by a factor (ICA +VA)/CCA = 0.745 (i.e., 74.5% of CCA to the IC compartment). However, this led to an undervaluation of the database IC flow compared to our reference [36]; so, it was decided to quit this reductive correction and the monolateral database CCA flow was just doubled and assumed as Φ_{ICA}. In this way the mean flow was 10.9±2.0 ml/s, with a good correspondence to Φ_{ICA} reported in [36]; i.e., (ICA + VA) = 11.7 ml/s.

Parameters R_{IC} and C_{ICA} were identified for each subject. The goodness of fit was given as usual by the percent of the predicted signal (i.e., AP) variance explained by the model. Results are given as median [1st, 3rd quartile] values.

The estimation of R_V was performed by setting the mean VP to a normal level of 10 mmHg. Briefly, the value of R_V was computed to fix the desired mean VP given the mean AP partition on the series of the previously determined R_{IC} and R_V itself.

Also, a virtually impaired Φ_{ICV} $R_V\uparrow$ was considered, fixing the mean VP at 20 mmHg. Given the small difference between mean VP and mean IC pressure, this setting was hypothesized to keep the latter in the borderline region without reaching pathological values [37]. Indeed, our focus was on a venous insufficiency likely to be below steady-state IC hypertension, yet sufficient to show significant effects on the VP pulsatility. The same WK parameters were kept with both the R_V and the $R_V\uparrow$ conditions.

The WK identification and its combination with either R_V or $R_V\uparrow$ performed on each of the 3325 subjects provided the overall statistics (median [1st quartile, 3rd quartile] of the $P_{ICV}(s)/P_{ICA}(s)$ TF parameters.

It is worth noting that the above was a two-stage approach. First, the WK parameters (R_{IC} and C_{ICA}) were estimated based on the virtual arterial data, and next a reasonable R_V value was introduced. A different valid approach could proceed in the opposite way considering $R_V + R_{IC}$ as a WK parameter in place of R_{IC} alone. The former approach was preferred since the venous pressure is commonly neglected in WK models model [11] given the low values of VP and R_V compared to AP and peripheral resistances, respectively.

2.4. Stratification by HR classes, statistics, and numerical simulations

The virtual database included simulations over three fixed heart period (HP) durations: i) tachycardic, HP = 831 ms, HR = 72.2 bpm, N = 1375 subjects (23.4%); ii) normal HR, HP = 956 ms, HR = 62.8 bpm, N = 1172 (35.3%); iii) bradycardic, HP = 1125 ms, HR = 53.3 bmp, N = 778 (23.4 %). The grand-average HR over the 3325 subjects is 64.5 bpm (1.07 Hz). Although a concentrated distribution is an artifact of the simulation design, its span is fairly representative of a normal population at rest. The fixed HP within each class permitted the synchronization of Φ_{ICA} and AP across subjects and the computation of median [1st quartile, 3rd quartile] waves. Hence, the WK identification was repeated on these waves in each HR class, looking for changing relationships among HR harmonics and the AP to VP TF edges.

Accordingly, time-domain numerical simulations were performed for each HR class separately by applying the relevant median Φ_{ICA} wave as input to the median [1st quartile, 3rd quartile] TF specific to the HR class, thus sizing the population dispersion.

3. Results

3.1. Model parameters based on the whole virtual database

The virtual population descriptive statistics (median [1st and 3rd quartile]) for systolic, diastolic and mean AP and mean Φ_{ICA} and for the IC WK parameters are summarized in Table 1. The median mean AP was 84.8 mmHg, and the mean Φ_{ICA} was 10.56 ml/s.

The IC WK identification gave a median time constant τ_{WK} of 0.195 s (median z_{WK} at 0.83 Hz), with median R_{ICA} = 7.72 mmHg s/ml and C_{ICA} = 0.0248 ml/mmHg. The goodness of fit ranged around 75%, which was considered sufficient since higher-order features were out of our scope.

It is worth noting that z_{WK} falls close to heart rate (HR, alias 1st pulse harmonic), thus the 2nd and the 3rd HR harmonics fall in the derivative MFB.

Assuming a mean VP equal to 10 mmHg in the normal condition and 20 mmHg in the $R_V\uparrow$ case, the median steady-state gain (G_{AV} = meanVP / meanAP) was 0.118 in the normal condition, and 0.236 for the $R_V\uparrow$ case. So, R_V resulted equal to 1.03 mmHg/ml and $R_V\uparrow$ equal to 2.38 mmHg/ml.

The median AP to VP TF P_{ICV}/P_{ICA} (2) is represented as a Bode plot (log–log) in Fig. 3, where the normal R_V and the $R_V\uparrow$ cases are shown. The low-frequency zero z_{WK} (0.83 Hz, independently from R_V) is placed slightly below the grand-average HR (1.07 Hz). The high-frequency AV-CC pole is equal to 6.2 Hz in the normal virtual case R_V, while it is 2.7 Hz in the $R_V\uparrow$ case.

Concerning the interplay with HR, and qualitatively anticipating the detailed harmonic analysis of the next paragraph, the main harmonic content was found up to the 3rd harmonic (i.e., 3 HR = 3.21 Hz). Hence, for R_V, it fell within the derivative MFB with a consistent margin from the full coupling HFB. Conversely, in $R_V\uparrow$ condition, the 3rd harmonic slightly trespassed into the full coupling HFB. In summary, the 1st pulse harmonic (i.e. at frequency equal to HR) challenges the veins by a water-hammer effect with no further attenuation compared to the DC gain G_{AV} (i.e. VP % pulsatility = AP % pulsatility). Furthermore, the 2nd and 3rd harmonics are even amplified compared to the 1st one, almost proportionally to their frequency, given the derivative characteristic. In $R_V\uparrow$, a similar spectral shape is kept, but multiplied by $R_V\uparrow/ R_V$, i.e., about 2-fold in our simulations. So, the model predicts a sharper upstroke due to the derivative MFB both in R_V and $R_V\uparrow$conditions. This phenomenon should be emphasized at higher HR and R_V values.

3.2. Time and frequency domain analysis in the three HR classes

Median and quartile waves are shown in Fig. 4, for each HR class. The respective results of IC WK identification are listed in Table 2. Interestingly, the shift of HR towards higher frequencies with tachycardia was almost proportionally followed by a frequency shift of the Bode plot edges z_{WK}, p_{AV}, and $p_{AV}\uparrow$, thus keeping common harmonic behaviors across the three HR classes.

Table 3 confirms that the harmonic amplitude is rapidly decreasing in all the HR classes, thus permitting to neglect harmonics above the 4th one. A broader harmonic content is shown by Φ_{ICA}, which is upstream to

Table 1
Identification of the intracranial (IC) arterial Windkessel (WK) parameters on the whole database of 3325 virtual subjects. Statistics as median [1st quartile, 3rd quartile]. From top to bottom: i) heart rate (HR) and number for the three HR classes; ii) hemodynamic values: systolic arterial pressure (SAP), diastolic arterial pressure (DAP), mean arterial pressure (MAP), mean flow (MFL); iii) WK identification results (R_{IC} = Intracranial Resistance; C_{ICA} = Intracranial arterial compliance; τ_{WK}= time constant; z_{WK}= IC WK pole (assuming the role of a zero); iv) arteriovenous capacitive coupling (AV-CC) parameters in normal venous resistance (R_V) condition (G_{AV} = arteriovenous capacitive coupling gain; p_{AV}=arteriovenous capacitive coupling pole); v) AV-CC parameters in increased venous resistance ($R_V\uparrow$) condition ($G_{AV}\uparrow$=arteriovenous capacitive coupling gain in $R_V\uparrow$ condition; $p_{AV}\uparrow$ =arteriovenous capacitive coupling pole in $R_V\uparrow$ condition).

i) HR [bpm] (No. of subjects)	Tachycardic 72.2 (1375) Normal HR 62.8 (1172) Bradychardic 53.3 (778) Total 64.5 (3325)	
ii) Hemodynamic values	SAP [mmHg]	116.5 [101.8, 131.2]
	DAP [mmHg]	56.7 [48.9, 66.9]
	MAP [mmHg]	84.8 [76.2, 95.9]
	MFL [ml/s]	10.6 [9.3, 12.4]
iii) WK identification results	R_{IC} [mmHg/(ml/s)]	7.72 [7.18, 8.30]
	C_{ICA} [ml/mmHg]	0.0248 [0.0189, 0.0345]
	τ_{WK} [s]	0.194 [0.135, 0.264]
	z_{WK} [Hz]	0.818 [0.602, 1.178]
iv) AV-CC parameters in R_V condition	R_V [mmHg/(ml/s)]	1.031 [0.875, 1.195]
	G_{AV} [adim]	0.118 [0.104, 0.131]
	p_{AV} [Hz]	7.06 [5.03, 10.34]
v) AV-CC parameters in $R_V\uparrow$ condition	$R_V\uparrow$ [mmHg/(ml/s)]	2.39 [1.99, 2.82]
	$G_{AV}\uparrow$ [adim]	0.236 [0.209, 0.262]
	$p_{AV}\uparrow$ [Hz]	3.53 [2.52, 5.17]

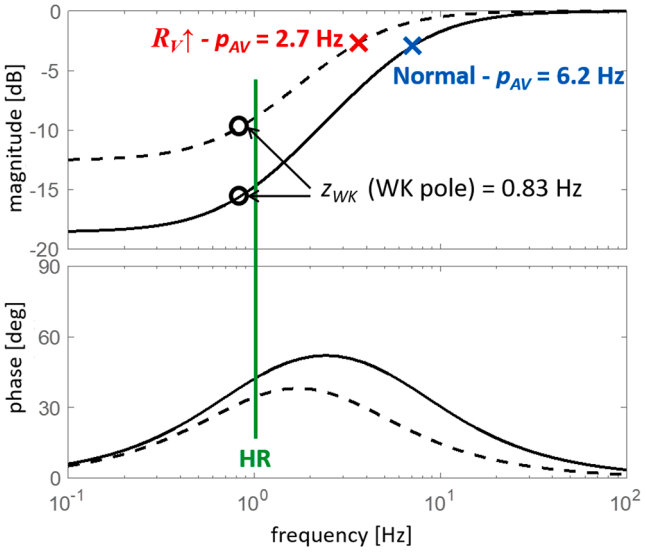

Fig. 3. Bode diagram of AP to VP TF (2). Median IC-WK parameters with normal (plain line) and increased ($R_V\uparrow$, dashed line) venous resistance. Position of the grand-average HR (green line). $p_{AV}\uparrow$ =arteriovenous capacitive coupling pole in $R_V\uparrow$ condition.

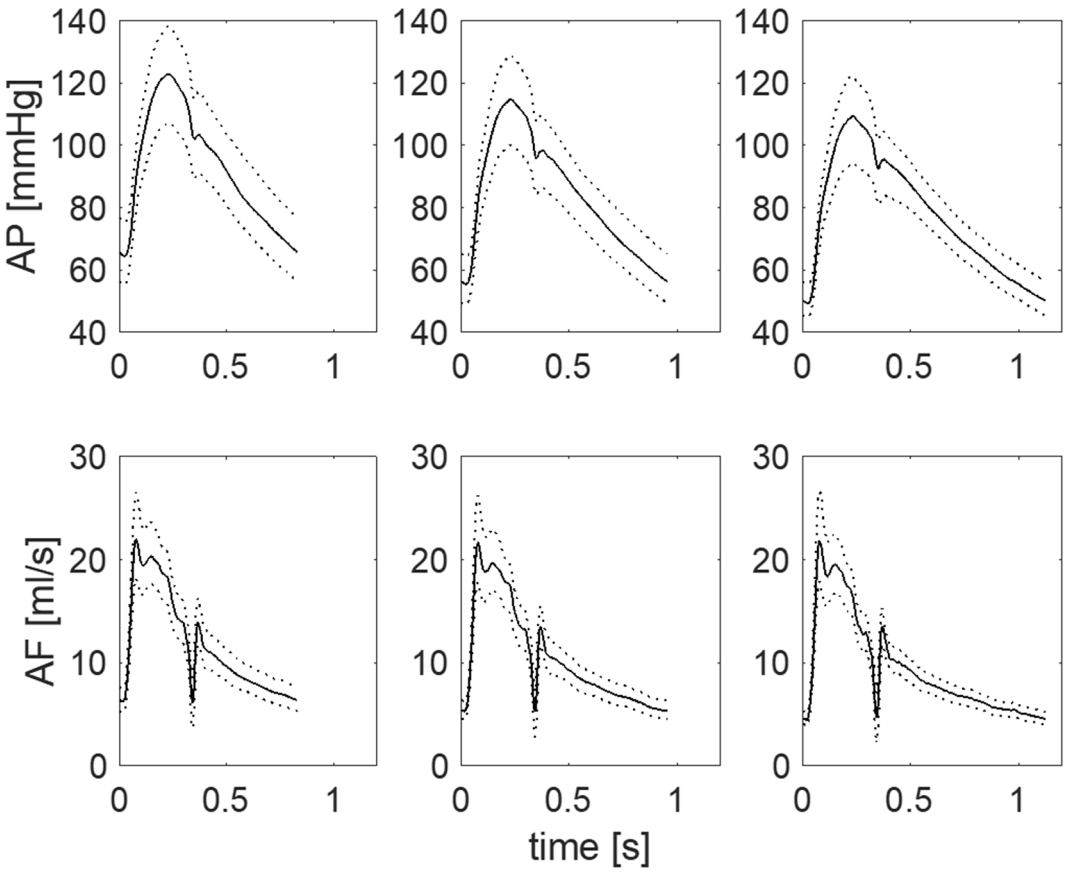

Fig. 4. Arterial pressure (AP, top) and flow (Φ_{ICA}, bottom) waves of tachycardic (left), normal HR (center), and bradycardic (right) classes. Median (plain line) with the 1st and 3rd quartile (dotted lines) waves are shown.

the WK low-pass filtering. Since the TF edges are shifting almost proportionally to the HR and its harmonics, the results qualitatively anticipated for the overall TF hold for each HR class. Namely, the 3 harmonics are within the derivative MFB, with the 3rd one at the edge with the HFB only for the $R_V\uparrow$ condition.

The interplay of harmonics and the Φ_{ICA} to VP TF is reflected by the time courses simulated in Fig. 5 for each HR class. Note also that the VP peak leads over the AP peak, as predicted by the derivative feature of the AV-CC.

4. Discussion

4.1. General outcomes of the theoretical modelling study

The mechanism of arterial sphygmic wave propagation to the IC venous compartment was modeled here starting from the minimal 2-element arterial WK, namely the compliance C_{ICA} and resistance R_{IC}. To account for the Monroe-Kelly hypothesis of a constant IC volume of incompressible fluids and tissues, the arterial WK was modified by the AV-CC exerted by C_{ICA} itself and modulated by the R_V. Thus a 3-element IC WK was proposed as a minimal model accounting for VP pulsatility, since the intracranial venous compliance satisfies the condition $C_{ICV} \gg C_{ICA}$ and was assimilated to a short circuit and accordingly neglected. So, the single C_{ICA} is pivoting both the WK and the AV-CC mechanisms. The proposed model is shown to provide some insight into AP to VP pulse propagation, yet with the huge simplifications discussed in the last paragraph.

Since IC pressure data can be estimated using invasive measures, the IC WK was estimated using an open database of 3325 virtual subjects [34] and the descriptive statistics of the identified C_{ICA} and R_{IC} parameters were presented in Table 1. Importantly, we named the single arterial WK pole as zero z_{WK}, given its role in the AV-CC coupling TF. The many parametric combinations relevant to the simulated virtual individuals are believed to represent the physiological variability of the human arterial system, thus allowing us to provide a descriptive statistic (median and quartiles) of the few addressed parameters. The database included tachycardic, normal HR, and bradycardic subjects, which allowed us to compare different positions of pulse harmonics with the edges of the respective TFs.

The effect of VP outflow resistance was simulated by imposing a mean VP of 10 mmHg, which should be congruent with a normal IC pressure, thus allowing us to estimate R_V. An $R_V\uparrow$ condition, simulating hindered Φ_{ICV} conditions such as chronic cerebrospinal venous insufficiency, was estimated by doubling the mean VP to 20 mmHg, which should be borderline to IC hypertension. As expected, $R_V\uparrow$ resulted to be about double compared to R_V.

The AP to VP TF was flat in the LFB, up to the WK pole, here assuming the role of a zero, z_{WK}. Hence, a MFB with derivative behavior was found, up to the AV-CC pole p_{AV}, which was the edge of the HFB where full-coupling (no attenuation from AP to VP) was reached. Accordingly, the 2-fold VP amplification due to $R_V\uparrow$ was kept in the LFB and up to the upper end of the MFB. However, the MFB was shrunk, since the AV-CC pole at $R_V\uparrow$ ($p_{AV}\uparrow$), was 2-fold lower than the normal p_{AV}. At higher frequencies, the $R_V\uparrow$ separation from R_V faded, since both conditions reached the HFB full coupling. The frequency analysis of AP and VP waves revealed a main harmonic content up to the first 3 harmonics, with the 1st one (HR) at the lower bound of the MFB and the upper harmonics within the MFB (or slightly trespassing into the HFB for $R_V\uparrow$). The consequences were that: i) no percent attenuation compared to the mean VP is experienced by the 1st harmonic; ii) higher harmonics are further amplified proportionally to their frequency and are also anticipated in their phase by the derivative MFB; iii) absolute pulse

Table 2
Analysis of median [1st quartile, 3rd quartile] waves in the tachycardic, normal heart rate (HR), and bradycardic HR classes. From top to bottom: *i*) hemodynamic values: systolic arterial pressure (SAP), diastolic arterial pressure (DAP), median arterial pressure (MAP), median flow (MFL); *ii*) Windkessel (WK) identification results; *iii*) arteriovenous capacitive coupling (AV-CC) parameters in R_V condition; *iv*) AV-CC parameters in $R_V\uparrow$ condition.

		Tachycardic HR = 72.2 bpm	Normal HR = 62.8 bpm	Bradycardic HR = 53.3 bpm
i)	SAP [mmHg]	122.9 [107.2, 138.1]	114.8 [100.0, 128.9]	109.2 [94.4, 122.2]
	DAP [mmHg]	64.4 [55.1, 75.2]	55.4 [48.7, 64.0]	49.3 [44.7, 55.4]
	MAP [mmHg]	92.4 [80.9, 105.1]	83.8 [73.7, 93.8]	77.2 [69.2, 84.9]
	MFL [ml/s]	11.7 [9.9, 13.7]	10.4 [8.9, 12.1]	9.5 [8.1, 10.8]
ii)	R_{IC} [mmHg/(ml/s)]	7.65 [7.89, 7.43]	7.73 [8.01, 7.45]	7.83 [8.14, 7.53]
	C_{ICA} [ml/mmHg]	0.0208 [0.0206, 0.0232]	0.0235 [0.0233, 0.0253]	0.0268 [0.0288, 0.0286]
	τ_{WK} [s]	0.159 [0.163, 0.172]	0.182 [0.186, 0.188]	0.210 [0.235, 0.215]
	z_{WK} [Hz]	0.998 [0.978, 0.923]	0.876 [0.854, 0.845]	0.759 [0.679, 0.739]
iii)	R_V [mmHg/(ml/s)]	0.928 [1.113, 0.781]	1.048 [1.257, 0.888]	1.165 [1.375, 1.005]
	G_{AV} [adim]	0.108 [0.124, 0.095]	0.119 [0.136, 0.107]	0.130 [0.144, 0.118]
	p_{AV} [Hz]	9.23 [7.92, 9.70]	7.34 [6.29, 7.93]	5.86 [4.70, 6.28]
iv)	$R_V\uparrow$ [mmHg/(ml/s)]	2.11 [2.59, 1.75]	2.42 [2.98, 2.02]	2.74 [3.31, 2.32]
	$G_{AV}\uparrow$ [adim]	0.216 [0.247, 0.190]	0.239 [0.271, 0.213]	0.259 [0.289, 0.235]
	$p_{AV}\uparrow$ [Hz]	4.61 [3.96, 4.85]	3.67 [3.15, 3.96]	2.93 [2.35, 3.14]

magnitudes are proportional to R_V (2-fold, in the simulated $R_V\uparrow$ condition); and iv) harmonic amplification would be increased in case of higher HR if the TF edges were not proportionally shifted.

Such detrimental effect of higher HRs on VP pulse, was not seen by comparing the three available HR classes, since the TF edges $|z_{WK}| < |p_{AV}\uparrow| < |p_{AV}|$ shifted almost proportionally to HR, keeping the overall relationships of $|z_{WK}| \approx$ HR, $|p_{AV}\uparrow| \approx 3$ HR, and $|p_{AV}| \approx 6$ HR. However, this behavior might be related to the virtual nature of the used database and requires confirmation on real data.

As to the counterintuitive VP pulse anticipation compared to the AP pulse due to the derivative MFB, such a prediction requires to be experimentally confirmed with a future specific study. However, it might represent a core element of AV-CC and play an important role in the venous depletion that favors Φ_{ICA} given the Monroe-Kelly constrain of confined IC volume.

The AV-CC mechanism is likely to play a major role in attenuating the "water-hammer" effect of Φ_{ICA} pulse, within the rigid IC compartment, since it favors in the fastest way the Φ_{ICV} needed to counterbalance the Φ_{ICA}. Hence, some VP pulsatility is physiologically needed and is a striking peculiarity of the IC compartment. However, the mechanism efficiency heavily relies on low R_V values and is hindered in $R_V\uparrow$ conditions, such as in chronic cerebrospinal venous insufficiency, in which a detrimental excess of IC VP pulsatility can be predicted.

4.2. Clinical impact

As to the possible link between extracranial venous impairment (such as in chronic cerebrospinal venous insufficiency) and neurodegeneration, our model showed that $R_V\uparrow$ may cause VP pulsatility increment, which may favor molecular leakage from venous blood to the brain interstitium. This may in turn trigger inflammation and the consequent neurodegeneration and leukoaraiosis [10]. Moreover, this effect is in keeping with the brain lesion development around IC vessels as described by the central vein sign in multiple sclerosis [38]. This study, though in a very simplified way, suggests that, aside from chronical imbalances of mean VP values, augmented pulsatile stress might challenge the IC vein walls, beat after beat through the many years leading to the clinical evidence of neurodegeneration. Although this model may theoretically explain these phenomena, it should be stressed that the present modelling study lacks experimental validation, which is presently difficult to achieve since it requires the contemporaneous recording of both vascular flows and pressures. Indeed, valid noninvasive measures of flows are available, e.g., by ultrasound or by phase-contrast MRI [18,39]. Conversely, the dynamic and precise measures of pressures would require highly invasive methods. In conclusion, the meaning of the present theoretical work, is to formulate hypothesis for future research studies. Moreover, complex and detailed models have been suggested for a better description of pathological cases [14].

A further clinically relevant effect predicted by the model is the reduced pulsatility across the brain vascular bed resistance R_{IC}, which effect is known to non-linearly augment the apparent value of the resistance itself [35], eventually hindering brain perfusion. For this reason, our model supports the hypothesis that higher R_V, via higher VP pulsatility, might be one of the causes of hypoperfusion. Hypoperfusion has been reported in various degenerative diseases [40–43], even related to R_V impairment [44] or hypertension and internal jugular veins reflux [45]. A very recent study [46] using near-infrared spectroscopy showed that internal jugular vein clamping caused a significant brain tissue oxygen saturation reduction, and cerebral hypoperfusion.

Finally, the focus posed on the interference between HR and pulsatile

Table 3
Harmonic analysis by heart rate (HR) class. Analysis of median [1st quartile, 3rd quartile] waves in the tachycardic, normal HR, and bradycardic HR classes. P-to-p = peak-to-peak; Φ_{ICA} = arterial flow; AP = Arterial pressure; VP = venous pressure; R_V = venous resistance; $R_V\uparrow$ increased venous resistance.

	Harmonic	Frequency	Φ_{ICA}	AP	VP, R_V	VP, $R_V\uparrow$	VP
			p-to-p	p-to-p	p-to-p	p-to-p	$R_V\uparrow$ / R_V
	#	[Hz]	[ml/s]	[mmHg]	[mmHg]	[mmHg]	[adim]
Tachycardic	1	1.20	7.57	33.68	5.66	11.04	1.95
	2	2.41	4.55	13.61	3.72	6.81	1.83
	3	3.61	2.47	5.95	2.25	3.80	1.69
	4	4.81	0.89	1.87	0.88	1.38	1.56
Normal HR	1	1.05	7.21	33.14	6.10	11.85	1.94
	2	2.09	4.50	14.04	4.17	7.54	1.81
	3	3.14	3.06	7.26	2.96	4.90	1.65
	4	4.18	1.23	2.72	1.37	2.09	1.52
Bradycardic	1	0.89	6.89	32.94	6.49	12.57	1.94
	2	1.78	4.34	14.02	4.42	7.90	1.79
	3	2.67	3.31	8.16	3.51	5.71	1.63
	4	3.56	2.13	4.34	2.30	3.42	1.49

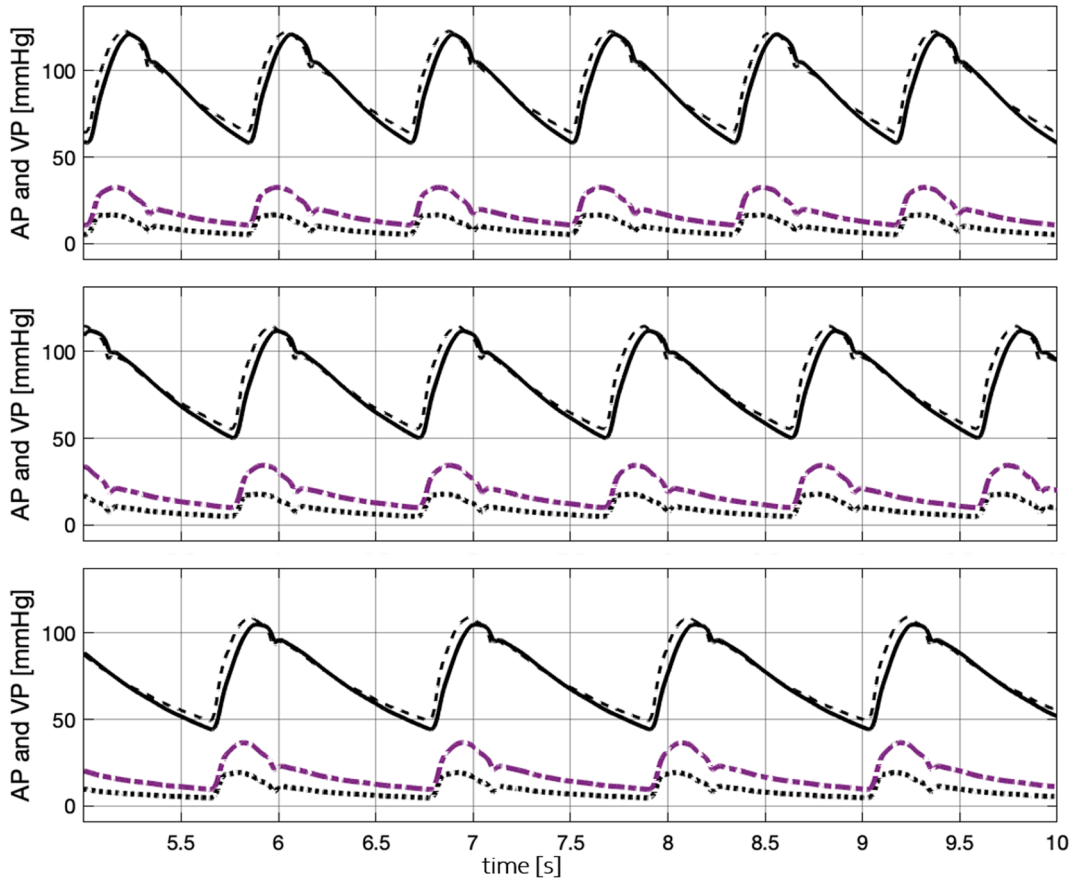

Fig. 5. Time domain simulation of tachycardic (top), normal HR (middle), and bradycardic (bottom) waves. Input was given by the median arterial flow (Φ_{ICA}) wave (not shown). Arterial pressure (AP) simulated by the Windkessel (WK) filter (plain line) and original median AP (dashed); venous pressure (VP) produced by the arteriovenous coupling (AV-CC) in the conditions of normal venous resistance (R_V, dotted line) and increased venous resistance ($R_V\uparrow$, dot-dash line). Note the almost double amplitude of $R_V\uparrow$ vs. R_V VP pulse and also the anticipation of both vs. AP. Simulation over 10 s, the first 5 discarded to reach periodical regime.

effects of hindered Φ_{ICV}, might impact rehabilitation protocols, since cardiovascular parameters can be normalized by suitable exercising. Conversely, interventional decreases of R_V have encountered many difficulties, so far. Further studies can hence address targeted rehabilitation protocols and, in this perspective, also the introduction of respiratory effects into the model is seen as a major point.

Indeed, several clinical contexts show comorbidities in which neurodegeneration is paralleled by cardiovascular conditions of increased HR. So, the combination of impaired Φ_{ICV} and increased HR as a risk factor deserves further investigation, in view of studies reporting HR-related cerebral damage [47].

4.3. Model limitations

This hyper-simplified model of AV pulse interactions is proposed to pinpoint some core relationships between the IC arterial WK, the venous resistances, and the harmonic content of the arterial pulse, in turn influenced by the HR. However, given the various simplifications, the model has some limits commented as follows. First, the extreme simplification of single arterial and venous lumped compartments misses important spatial and dynamic features. This limitation is particularly important considering the IC veins and sinuses network complexity, which is conversely addressed by sophisticated models such as that of Muller and Toro [25], supported by flow measures via Phase-Contrast Magnetic Resonance Imaging. In line with previous studies [48], these authors highlight the importance of Starling resistors between central veins and their drainage into the dural sinuses. The resulting pressure drop is shown to be essential to the CSF production/reabsorption cycle and, ultimately, to IC pressure regulation and its pathological impairments [49].

Second, another main limitation of our model is not including the buffering effect due to the CSF and craniospinal compliance. Indeed, many studies do address CSF dynamics and stress the importance of its interactions with the arterial and venous compartments [3,25,26,50]. However, important models [3,26] of CSF behavior stem on the instantaneous imbalance between the arterial and the venous flow, thus neglecting the interactions between the two vascular compartments focused by the proposed simple model. Rather, we separately addressed the AP to VP waves and their interactions inside the IC compartment, possibly upstream to the CSF buffering effect. The proposed AV-CC concept, however, is still a theoretical model-based prediction, which requires future experimental validation. This aim addresses pressure features in internal IC veins, which could be directly solved only via highly invasive measures or by indirect computations by non-trivial fluid-dynamic models. The same ought to be said relevant to the WK parameter estimation, at this stage limited to the analysis of a virtual database.

Finally, in this first approach, we neglected factors influencing the Φ_{ICV} and pressure such as the thoracic pump [39,51 52] and the posture [39,53], that are known to significantly change the outflow routes and dynamics [27]. Also, the potent autoregulation mechanisms [54], known to continuously stabilize brain perfusion against external perturbations, such as AP changes, were not considered at this stage. These elements would be of major clinical and rehabilitation impact and deserve to be considered in future studies.

5. Conclusion

The proposed theoretical modelling approach provides, in the simplest way, future working hypotheses about the interaction between arteriovenous coupling and a lumped R_V, which hinders the IC volume balance and generates a VP pulse proportional to the resistance itself. However, the extreme lumping misses any localization of mechanisms inside the complex IC system of veins and sinuses. Thus, further experimental investigation is needed as well as reference to more detailed models to assess the role of the highlighted dynamic mechanisms. So far, the clinical focus has been given to static (alias, mean hemodynamic values) chronic effects on IC circulation. This study, conversely, broadens the attention to the IC dynamics, which in turn recalls its dialogue with the dynamics of the whole systemic cardiovascular and cardiorespiratory functions.

CRediT authorship contribution statement

Giuseppe Baselli: Conceptualization, Data curation, Formal analysis, Methodology, Software, Validation, Visualization, Writing – original draft, Writing – review & editing. **Maria Marcella Laganà:** Conceptualization, Writing – original draft, Writing – review & editing.

Declaration of Competing Interest

The authors declare that they have no known competing financial interests or personal relationships that could have appeared to influence the work reported in this paper.

Acknowledgements

This study was partially funded by the Italian Ministry of Health "Ricerca Corrente" and by the Lombardy Region (Announcement No. POR-FESR 2014-2020) within the project named "Sistema Integrato DomiciliarE e Riabilitazione Assistita al Benessere" (SIDERA^B). We thank Dr. Paul Kokeny (SpinTech Inc., Bingham Farms, MI, USA) for the English language revision.

References

[1] R. Zivadinov, Is there a link between the extracranial venous system and central nervous system pathology? BMC Med 11 (2013) 259.
[2] N. Kuriyama, T. Tokuda, J. Miyamoto, N. Takayasu, M. Kondo, M. Nakagawa, Retrograde jugular flow associated with idiopathic normal pressure hydrocephalus, Ann Neurol 64 (2008) 217–221.
[3] N. Alperin, B.L. Lam, R.W. Tain, S. Ranganathan, M. Letzing, M. Bloom, B. Alexander, P.R. Aroucha, E. Sklar, Evidence for altered spinal canal compliance and cerebral venous drainage in untreated idiopathic intracranial hypertension, Acta Neurochir Suppl 114 (2012) 201–205.
[4] K. Han, H.H. Hu, A.C. Chao, F.C. Chang, C.P. Chung, H.Y. Hsu, W.Y. Sheng, J. Wu, Transient Global Amnesia Linked to Impairment of Brain Venous Drainage: An Ultrasound Investigation, Front Neurol 10 (2019) 67.
[5] G. Attanasio, L. Califano, A. Bruno, V. Giugliano, M. Ralli, S. Martellucci, C. Milella, M. de Vincentiis, F.Y. Russo, A. Greco, Chronic cerebrospinal venous insufficiency and meniere's disease: Interventional versus medical therapy, Laryngoscope 130 (2020) 2040–2046.
[6] C. Zhang, B. Wu, X. Wang, C. Chen, R. Zhao, H. Lu, H. Zhu, B. Xue, H. Liang, S. K. Sethi, E.M. Haacke, J. Zhu, Y. Peng, J. Cheng, Vascular, flow and perfusion abnormalities in Parkinson's disease, Parkinsonism Relat Disord 73 (2020) 8–13.
[7] D. Jakimovski, M. Topolski, K. Kimura, V. Pandya, B. Weinstock-Guttman, R. Zivadinov, Decrease in Secondary Neck Vessels in Multiple Sclerosis: A 5-year Longitudinal Magnetic Resonance Angiography Study, Curr Neurovasc Res 16 (2019) 215–223.
[8] G.D.E. Papini, G. Di Leo, M. Zanardo, M.P. Fedeli, I. Merli, F. Sardanelli, Measurement of jugular foramen diameter using MRI in multiple sclerosis patients compared to control subjects, Eur Radiol Exp 1 (2017) 4.
[9] M. Simka, M. Skula, Potential Involvement of Impaired Venous Outflow from the Brain in Neurodegeneration: Lessons Learned from the Research on Chronic Cerebrospinal Venous Insufficiency, Rev Recent Clin Trials 14 (2019) 235–236.
[10] D. Nan, Y. Cheng, L. Feng, M. Zhao, D. Ma, J. Feng, Potential Mechanism of Venous System for Leukoaraiosis: From post-mortem to in vivo Research, Neurodegener Dis 19 (2019) 101–108.
[11] N. Westerhof, J.-W. Lankhaar, B.E. Westerhof, The arterial Windkessel, Med Biol Eng Comput 47 (2) (2009) 131–141.
[12] C.C. Mei, J. Zhang, H.X. Jing, Fluid mechanics of Windkessel effect, Med Biol Eng Comput 56 (8) (2018) 1357–1366.
[13] N. Westerhof, F. Bosman, C.J. De Vries, A. Noordergraaf, Analog studies of the human systemic arterial tree, J Biomech 2 (2) (1969) 121–143.
[14] P.J. Blanco, L.O. Müller, S.M. Watanabe, R.A. Feijóo, On the anatomical definition of arterial networks in blood flow simulations: comparison of detailed and simplified models, Biomech Model Mechanobiol 19 (5) (2020) 1663–1678.
[15] G.A. Bateman, C.R. Levi, P. Schofield, Y. Wang, E.C. Lovett, The venous manifestations of pulse wave encephalopathy: windkessel dysfunction in normal aging and senile dementia, Neuroradiology 50 (6) (2008) 491–497.
[16] M. Ursino, C.A. Lodi, A simple mathematical model of the interaction between intracranial pressure and cerebral hemodynamics, J Appl Physiol 82 (1997) (1985) 1256–1269.
[17] M. Ursino, A mathematical study of human intracranial hydrodynamics. Part 1–The cerebrospinal fluid pulse pressure, Ann Biomed Eng 16 (1988) 379–401.
[18] A. Wåhlin, K. Ambarki, J. Hauksson, R. Birgander, J. Malm, A. Eklund, Phase contrast MRI quantification of pulsatile volumes of brain arteries, veins, and cerebrospinal fluids compartments: repeatability and physiological interactions, J Magn Reson Imaging 35 (5) (2012) 1055–1062.
[19] D. Greitz, Cerebrospinal fluid circulation and associated intracranial dynamics. A radiologic investigation using MR imaging and radionuclide cisternography, Acta Radiol Suppl 386 (1993) 1–23.
[20] M.M. Laganà, S.J. Shepherd, P. Cecconi, C.B.J.B.S.P. Beggs. Control, Intracranial volumetric changes govern cerebrospinal fluid flow in the Aqueduct of Sylvius in healthy adults. 36. 2017. 84-92.
[21] W. Wakeland, B. Goldstein, A review of physiological simulation models of intracranial pressure dynamics, Comput Biol Med 38 (9) (2008) 1024–1041.
[22] A. Ficola, M.L. Fravolini, C. Anile, A physical model of the intracranial system for the study of the mechanisms of the cerebral blood flow autoregulation, IEEEAccess 6 (2018) 67166–67175.
[23] K. Ambarki, O. Baledent, G. Kongolo, R. Bouzerar, S. Fall, M.-E. Meyer, A new lumped-parameter model of cerebrospinal hydrodynamics during the cardiac cycle in healthy volunteers, IEEE Trans Biomed Eng 54 (3) (2007) 483–491.
[24] G. Gadda, A. Taibi, F. Sisini, M. Gambaccini, P. Zamboni, M. Ursino, A new hemodynamic model for the study of cerebral venous outflow, Am J Physiol Heart Circ Physiol 308 (3) (2015) H217–H231.
[25] L.O. Müller, E.F. Toro, Enhanced global mathematical model for studying cerebral venous blood flow, J Biomech 47 (13) (2014) 3361–3372.
[26] R.-W. Tain, N. Alperin, Noninvasive intracranial compliance from MRI-based measurements of transcranial blood and CSF flows: indirect versus direct approach, IEEE Trans Biomed Eng 56 (3) (2009) 544–551.
[27] P. Mohammadyari, G. Gadda, A. Taibi, Modelling physiology of haemodynamic adaptation in short-term microgravity exposure and orthostatic stress on Earth, Sci Rep 11 (2021) 4672.
[28] P. Mohammadyari, G. Gadda, A. Taibi, J. Munuera Del Cerro, Paediatric haemodynamic modelling: development and experimental validation using quantitative flow MRI, Eur Radiol Exp 4 (2020) 16.
[29] L.O. Muller, E.F. Toro, E.M. Haacke, D. Utriainen, Impact of CCSVI on cerebral haemodynamics: a mathematical study using MRI angiographic and flow data, Phlebology 31 (2016) 305–324.
[30] S. Marcotti, L. Marchetti, P. Cecconi, E. Votta, G.B. Fiore, A. Barberio, S. Viotti, A. Redaelli, M.M. Lagana, An anatomy-based lumped parameter model of cerebrospinal venous circulation: can an extracranial anatomical change impact intracranial hemodynamics? BMC Neurol 15 (2015) 95.
[31] E.F. Toro, Computation, Brain venous haemodynamics, neurological diseases and mathematical modelling. A review, J Applied Mathematics 272 (2016) 542–579.
[32] G. Baselli, P. Arrigoni, M. Boles, E. Mikhaeil, F. Tawadrous, M.M.J.V. Laganà. Lymphatics, Hyper-simplified cerebrovascular model: high sensitivity of venous pulsatility vs venous resistance. 2019.
[33] G. Baselli M.M. Laganà T.S. Cerebrovascular. Windkessel: A Simplified Model. In: 11th Conference of the European Study Group on Cardiovascular Oscillations (ESGCO). IEEE. 2020. 2020. 1-2.
[34] Marie Willemet, Phil Chowienczyk, Jordi Alastruey, A database of virtual healthy subjects to assess the accuracy of foot-to-foot pulse wave velocities for estimation of aortic stiffness, Am J Physiol Heart Circ Physiol 309 (4) (2015) H663–H675.
[35] F. Aletti, G. Baselli, Model study of the effects of interactions between systemic and peripheral circulation on interstitial fluid balance, J Gravit Physiol 14 (2007) P51–52.
[36] M. Schoning, J. Walter, P. Scheel, Estimation of cerebral blood flow through color duplex sonography of the carotid and vertebral arteries in healthy adults, Stroke 25 (1994) 17–22.
[37] L. Rangel-Castilla, S. Gopinath, C.S. Robertson, Management of intracranial hypertension, Neurol Clin 26 (2008) 521–541.
[38] A. Bhandari, H. Xiang, J. Lechner-Scott, M. Agzarian. Central vein sign for multiple sclerosis: A systematic review and meta-analysis. Clin Radiol, 75. 2020. 479. e479-479. e415.
[39] M.M. Lagana, M. Di Rienzo, F. Rizzo, C. Ricci, S. D'Onofrio, L. Forzoni, P. Cecconi, Cardiac, Respiratory and Postural Influences on Venous Return of Internal Jugular and Vertebral Veins, Ultrasound Med Biol 43 (2017) 1195–1204.
[40] M.M. Lagana, L. Pelizzari, F. Baglio, Relationship between MRI perfusion and clinical severity in multiple sclerosis, Neural Regen Res 15 (2020) 646–652.
[41] L. Pelizzari, S. Di Tella, F. Rossetto, M.M. Lagana, N. Bergsland, A. Pirastru, M. Meloni, R. Nemni, F. Baglio, Parietal Perfusion Alterations in Parkinson's Disease Patients Without Dementia, Front Neurol 11 (2020) 562.
[42] Dongxue Li, Yuancheng Liu, Xianchun Zeng, Zhenliang Xiong, Yuanrong Yao, Daiyi Liang, Hao Qu, Hui Xiang, Zhenggui Yang, Lisha Nie, Pu-Yeh Wu,

Rongpin Wang, Quantitative Study of the Changes in Cerebral Blood Flow and Iron Deposition During Progression of Alzheimer's Disease, J Alzheimers Dis 78 (1) (2020) 439–452.
[43] D. Jakimovski, M. Topolski, A.V. Genovese, B. Weinstock-Guttman, R. Zivadinov, Vascular aspects of multiple sclerosis: emphasis on perfusion and cardiovascular comorbidities, Expert Rev Neurother 19 (2019) 445–458.
[44] P. Zamboni, E. Menegatti, B. Weinstock-Guttman, M.G. Dwyer, C.V. Schirda, A. M. Malagoni, D. Hojnacki, C. Kennedy, E. Carl, N. Bergsland, C. Magnano, I. Bartolomei, F. Salvi, R. Zivadinov, Hypoperfusion of brain parenchyma is associated with the severity of chronic cerebrospinal venous insufficiency in patients with multiple sclerosis: a cross-sectional preliminary report, BMC Med 9 (2011) 22.
[45] J.C.L. Rodrigues, G. Strelko, E.A.H. Warnert, A.E. Burchell, S. Neumann, L.E. K. Ratcliffe, A.D. Harris, B. Chant, R. Bowles, A.K. Nightingale, R.G. Wise, J.F. R. Paton, E.C. Hart, Retrograde blood flow in the internal jugular veins of humans with hypertension may have implications for cerebral arterial blood flow, Eur Radiol 30 (2020) 3890–3899.
[46] S. Spagnolo, P. Spagnolo, L. Barbato, M. Grasso, P. Bavera, A. Carrozzo, R. Vardanyan, A. Arjomandi Rad. IThe Chronic Stenosis of the Internal Jugular Veins as a Cause of Multiple Sclerosis. Jorunal of Cardiology Research Reviews & Reports. SRC/JCDRR/106. J Cardiol Res Rev Rep. 2020.
[47] M. Nagai, S. Hoshide, K. Kario, The insular cortex and cardiovascular system: a new insight into the brain-heart axis, J Am Soc Hypertens 4 (2010) 174–182.
[48] J.M. Luce, J.S. Huseby, W. Kirk, J. Butler, A Starling resistor regulates cerebral venous outflow in dogs, J Appl Physiol Respir Environ Exerc Physiol 53 (1982) 1496–1503.
[49] R. De Simone, A. Ranieri, V. Bonavita, Starling resistors, autoregulation of cerebral perfusion and the pathogenesis of idiopathic intracranial hypertension, Panminerva Med 59 (2017) 76–89.
[50] C.B. Beggs, S.J. Shepherd, P. Cecconi, M.M. Lagana, Predicting the aqueductal cerebrospinal fluid pulse: a statistical approach, Applied Science 9 (2019) 2131.
[51] P. Zamboni, E. Menegatti, L. Pomidori, S. Morovic, A. Taibi, A.M. Malagoni, A. L. Cogo, M. Gambaccini, Does thoracic pump influence the cerebral venous return? J Appl Physiol 112 (2012) (1985) 904–910.
[52] Q. Zhang, M. Roche, K.W. Gheres, E. Chaigneau, R.T. Kedarasetti, W.D. Haselden, S. Charpak, P.J. Drew, Cerebral oxygenation during locomotion is modulated by respiration, Nat Commun 10 (2019) 5515.
[53] N. Alperin, S.G. Hushek, S.H. Lee, A. Sivaramakrishnan, T. Lichtor, MRI study of cerebral blood flow and CSF flow dynamics in an upright posture: the effect of posture on the intracranial compliance and pressure, Acta Neurochir Suppl 95 (2005) 177–181.
[54] R.B. Panerai, Cerebral autoregulation: from models to clinical applications, J Cardiovascular Engineering 8 (2008) 42–59.